Time intermittency in nondiffusive transport regimes of suprathermal ions in turbulent plasmas

F. Manke,* M. Baquero-Ruiz, I. Furno, O. Chellaï, A. Fasoli, and P. Ricci
École Polytechnique Fédérale de Lausanne (EPFL), Swiss Plasma Center (SPC), CH-1015 Lausanne, Switzerland

(Received 5 November 2018; published 29 May 2019)

Intermittent phenomena have long been studied in the context of nondiffusive transport across a variety of fields. In the TORPEX device, the cross-field spreading of an injected suprathermal ion beam by electrostatic plasma turbulence can access different nondiffusive transport regimes. A comprehensive set of suprathermal ion time series has been acquired, and time intermittency quantified by their skewness. Values distinctly above background level are found across all observed transport regimes. Intermittency tends to increase toward quasi- and superdiffusion and for longer propagation times of the suprathermal ions. The specific prevalence of intermittency is determined by the meandering motion of the instantaneous ion beam. We demonstrate the effectiveness of an analytical model developed to predict local intermittency from the time-average beam. This model might thus be of direct interest for similar systems, e.g., in beam physics, or meandering flux-rope models for solar energetic particle propagation. More generally, it illustrates the importance of identifying the system-specific sources of time-intermittent behavior when analyzing nondiffusive transport.

DOI: 10.1103/PhysRevE.99.053208

I. INTRODUCTION

The motion of a single particle or a collection of particles (such as fluid elements) is often termed *intermittent* in time when it features extended waiting times between brief, irregular occurrences of strong activity. Particularly in turbulence, the formation of distinct coherent structures has long been characterized as time-intermittent [1,2], and structures of high vorticity can be found to occur in spatially intermittent patches [3]. When considering a distribution of particles, time-intermittent behavior and the associated non-Gaussian statistics of particle motion can result in a nonlinear scaling of the particle mean-square displacement with time, $\langle \Delta x^2 \rangle \sim t^{\nu}$, with $\nu \neq 1$ [4–6]. Different aspects of time intermittency have therefore been investigated in relation to *nondiffusive* transport in a variety of scientific domains and contexts.

In random-walk-based transport models, the heavy-tailed waiting-time distributions often lead toward subdiffusion ($\nu < 1$) [4,7,8]. Intermittency in subdiffusive transport has been studied in areas ranging from space physics [9] to material aging [10] or sediment transport [11,15]. Superdiffusion ($\nu > 1$) can only arise from a competition with heavy-tailed jump length distributions [4]. Intermittency in superdiffusive transport has been reported, e.g., in conjunction with the formation of coherent structures in atmospheric [12] or plasma turbulence [13–15]. In purely mathematical studies, it has been demonstrated that any regime of nondiffusive transport can be generated through intermittency in simple functional mappings [16–18]. Likewise, certain biological systems can exhibit either super- or subdiffusive behavior as a result of intermittent motion [19]. However, the general question of whether super- or subdiffusion can be inferred from local observations of time intermittency has remained open.

In this paper, we investigate time intermittency in the motion of suprathermal ions with energies of 30–70 eV that are injected into the cold, turbulent plasmas of the TORoidal Plasma Experiment (TORPEX; see Fig. 1) [20–22]. The spreading of this comparatively "fast" ion beam exhibits a smooth transition between super-, quasi-, and subdiffusive transport regimes [23,24]. As direct measurements on single particles are not feasible, we quantify the intermittency of the fast ion beam motion by acquiring local fast ion time series and measure their skewness. Using first three-dimensional sets of such time series, we systematically quantify the prevalence of time intermittency across all the observed nondiffusive transport regimes. We furthermore introduce an analytical model [25] for the ion beam motion, which allows us to predict the skewness of these time series across various transport regimes, based solely on their local time-average (mean) value.

The paper is organized as follows: Sec. II introduces the TORPEX device in detail, with a focus on the fast ion experiments. In Sec. III, we present the principal experimental measurements of the ion beam and time intermittency across different nondiffusive transport regimes. Section IV adapts the analytical model we developed in [25] and demonstrates its predictive effectiveness by fitting predicted time-series statistics to the measurements. Finally, we summarize our findings in Sec. V.

II. EXPERIMENTAL METHODS

A. The TORPEX device

TORPEX is a basic plasma physics device, with major radius $R_0 = 1$ m and minor radius $a = 0.2$ m, featuring helical open magnetic field lines. Our experimental setup and coordinate convention are shown in Fig. 1.

The toroidal field on-axis is $B_\Phi = 74$ mT and the vertical field $B_v \approx 2$ mT, leading to a magnetic pitch angle of $\lesssim 2^\circ$.

*fabian.manke@epfl.ch

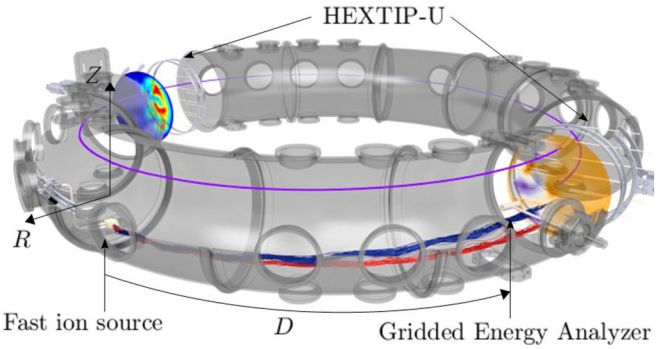

FIG. 1. Fast ion experimental setup in TORPEX. The poloidal coordinates R and Z are indicated, with $R = Z = 0$ on axis and the toroidal source-detector distance D. The gridded energy analyzer (GEA) can be displaced over most of the poloidal cross section. Fast ion trajectories are shown in red for an injection energy E of 30 eV, and in dark blue for 70 eV. A magnetic field line is indicated in purple. A plasma density profile interpolated from ion-saturation current measurements with the Langmuir probe arrays HEXTIP-U [26] is shown on the left, and its floating potential profile is shown on the right.

A hydrogen plasma with temperatures of $T_e \approx 2.5$ eV and $T_i < 1$ eV (for electrons and ions, respectively) and densities $n_e = n_i \approx 10^{16}$ m^{-3} is generated through microwave injection at 2.45 GHz, which lies in the electron-cyclotron (EC) range [27]. With the EC resonance layer on the high-field side (HFS) typically at $R \approx -12$ cm and a nearby upper hybrid resonance, strong density fluctuations from an interchange mode are present near $R \approx -10$ cm due to the radial density and temperature gradients [28–30]. This mode is the source of strong electrostatic plasma turbulence toward the center of the device. Intermittently, coherent field-aligned structures (so-called "blobs") [20,31,32] are generated. These blobs propagate toward the low-field side (LFS) due to their dipolelike nature and the associated $\mathbf{E}\times\mathbf{B}$ drift [31–33]. This well-characterized plasma scenario is the starting point for the study of nondiffusive fast ion transport.

B. Fast ion studies

Suprathermal ions are injected toroidally by thermal emission from a lithium-6 ion source delivering ≈10 μA of ion current under bias. The bias of the source itself as well as two successive grids is set to maintain the injected current while accelerating the ions in the toroidal direction to energies E of typically either 30 or 70 eV, and thus produce a beam of ions that can be considered as "fast" compared to the hydrogen plasma. The ion source is mounted at $R = -1$ cm and $Z = -14.5$ cm on a movable sleigh allowing the toroidal source-detector distance D to range from 126 to 171 cm. The detector is a dedicated back-to-back gridded energy analyzer (GEA), biased to filter out bulk electrons and ions [34] (see Fig. 1). After amplification, the back-side signal is subtracted from the front-side to reduce noise. Fast ions drift vertically due to the magnetic pitch angle, gradient, and curvature drifts. Turbulent electric fields affect the propagation of fast ions through localized $\mathbf{E}\times\mathbf{B}$ drifts [24,35].

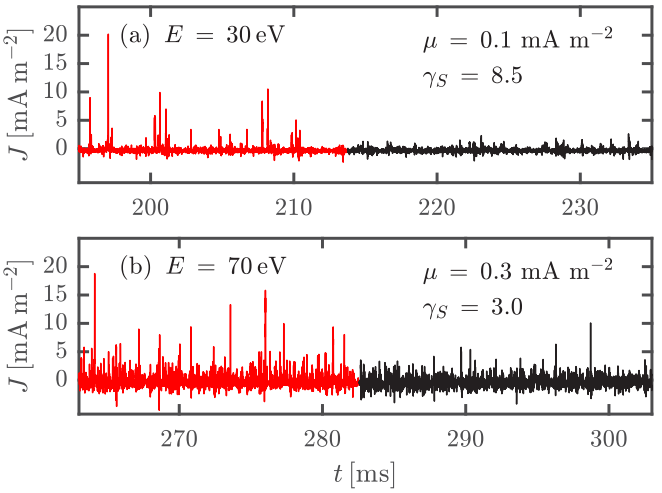

FIG. 2. Segments of the local time series of fast ion current density $J(t)$ that feature the highest skewness at $D = 171$ cm and respective energy. The ion-source on-phases are indicated in red, and the off-phases are in black. Distinct peaks are visible during the on-phase. The on-phase mean μ and skewness γ_S are given. For the mean, the off-phase value was subtracted. The locations (R, Z) of the GEA where these time series were collected are marked in Fig. 3.

Previous experiments [35] and theoretical studies [24] using fluid tracer simulations with the Global Branginskii Solver [23,30] have identified the nondiffusive regimes of the turbulent fast ion transport across magnetic field lines. With fast ion injection energies of $E = 30$ or 70 eV, at an injection angle of ≈6° to the toroidal direction, the average fast ion Larmor radii amount to ≈5 mm and ≈8 mm, respectively. Gyro- and drift averaging over the turbulent electric fields are therefore stronger at $E = 70$ eV. After a brief ballistic transport phase, this leads to *subdiffusion* at all D considered here. For 30 eV ions, superdiffusion occurs instead, which smoothly transitions to quasidiffusion around $D \gtrsim 100$ cm. At $D \geqslant 126$ cm, we therefore associate $E = 30$ eV with a *super- to quasidiffusive* regime. During initial studies in superdiffusion, transport appeared locally time-intermittent as certain fast ion time series showed significant skewness [14].

To generate such fast ion time series, as shown in Fig. 2, the GEA signal is sampled for 1.5 s at a frequency of 250 kHz. Consistent with previous publications, the measured currents are divided by the circular detector area with $d = 8$ mm and thus presented as local fast ion current density time series $J(t)$ at coordinates (R, Z). While the effective detector area may differ from this geometric estimate, this will only affect estimates for the total fast ion current I when used in Sec. IV, and compared to the conventions and fits in [25]. The ion source undergoes on and off cycles at 23 Hz to distinguish the fast ion signal from residual noise.

Time intermittency is quantified by each time series' skewness (Fisher-Pearson coefficient [36]), as distinct, intermittent peaks in the signal strongly affect the higher-order moments [2] (see Fig. 2). Kurtosis has thus been investigated as well, which leads to very similar observations. Hence, we focus on skewness in the following.

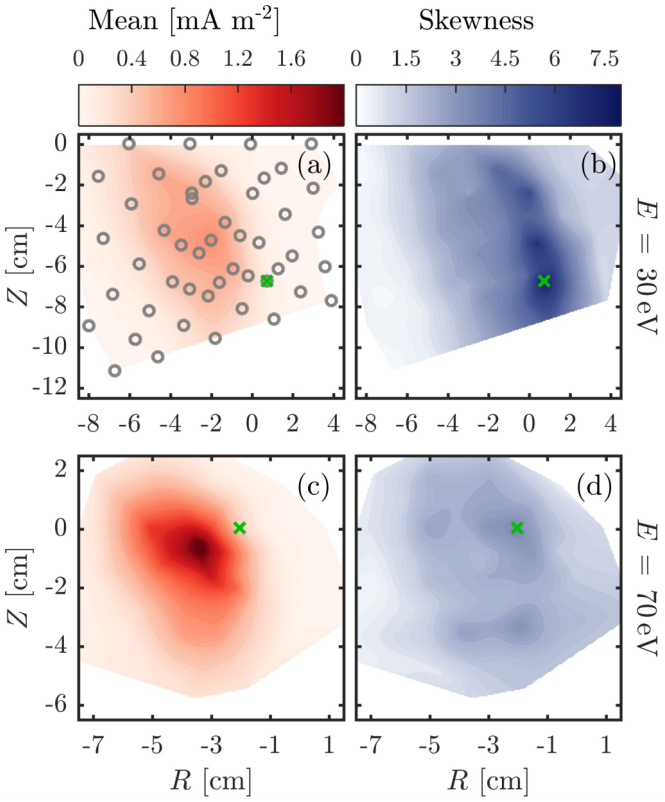

FIG. 3. Normalized mean and skewness profiles at $D = 171$ cm. Note the larger spread and reduced vertical drift at $E = 30$ eV, as well as the lower peak current density and higher maximum skewness. The gray circles in (a) indicate detector positions, and green crosses denote the positions at which the time-series samples in Fig. 2 were acquired. The noise contributions from the background plasma increase significantly toward the interchange mode on the HFS, and reduce the on-phase skewness here compared to the LFS.

III. RESULTS

We compute, for given D and E, poloidal mean and skewness profiles (see Fig. 3) to quantify intermittency. For the mean profiles, the time average of $J(t)$ during the on-phases of the modulated ion source is computed at each poloidal location (R, Z) and the local off-phase average subtracted, to compensate for acquisition offsets. The profile is then interpolated. The skewness profiles are interpolated directly over the on-phase signal skewness γ_S. For comparison, off-phase (noise) skewness never exceeds $\gamma_N \approx 2$. We also investigated a noise-reduced skewness γ_J for statistically independent signal and noise,

$$\gamma_J = \frac{\sigma_S^3\gamma_S - \sigma_N^3\gamma_N}{\left(\sigma_S^2 - \sigma_N^2\right)^{3/2}}, \tag{1}$$

where σ_S denotes the standard deviation of the on-phase signal, and σ_N that of the off-phase signal. However, this quantity quickly diverges in regions with a low signal, so that γ_S, the on-phase skewness, remains the measure for intermittency in what follows.

In practice, the total fast ion current I varies between profiles, depending on ion energy and source quality. This clearly affects the relative importance of contributions from the fast ions and noise to γ_S from one profile to the next. To allow a direct comparison between them, I is therefore estimated by numerically integrating the mean profile, and all mean and skewness profiles are then normalized to an averaged total current of $I_c = 2.85\ \mu$A (i.e., we "map" $\mapsto$),

$$J \mapsto cJ, \quad \gamma_S \mapsto \frac{c^3\sigma_S^3\gamma_S + (1-c^3)\sigma_N^3\gamma_N}{\left[c^2\sigma_S^2 + (1-c^2)\sigma_N^2\right]^{3/2}}, \tag{2}$$

where we use the normalization factor $c = \frac{I_c}{I}$. Note that if we normalized with $I_c \gg I$ (i.e., toward an arbitrarily strong signal), one would find $\gamma_S \mapsto \gamma_J$ as expected.

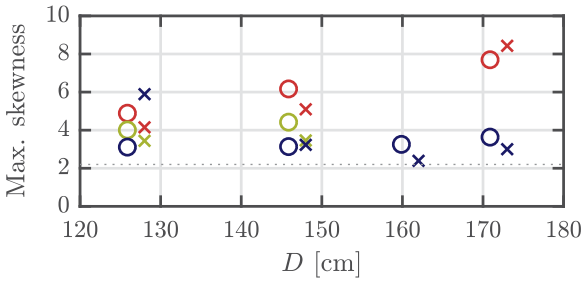

FIG. 4. Maximum normalized skewness for different source-detector distances D and fast ion energies E of 30, 50, and 70 eV in red, yellow, and dark blue (circles, top to bottom), respectively. Crosses show values before normalization [see Eq. (2)] and are offset by $D = +2$ cm for clarity. The dotted line indicates the maximum background value of $\gamma_N = 2.2$.

As summarized in Fig. 4, the normalized skewness is above the background (off-phase) level in many positions across all profiles. Lower energies show higher skewness, especially for longer D. Likewise, skewness increases further out in the LFS, provided the fast ions penetrate there measurably.

Especially for the 30 eV ions, the observed trends reflect the presence of distinct, intermittent peaks, which become increasingly rare toward the edges of the mean profile (see Fig. 2). As these peaks are most frequent near the maximum of the mean profile, they become less prominent compared to the local mean, which in turn limits the skewness there. These distinct peaks in fast ion current density consistently indicate that the fast ion beam at a given instant is more concentrated than its mean profile, especially for $E = 30$ eV.

IV. ANALYTICAL MODELING

Based on these characteristics of the fast ions, we have developed an analytical model for a setting in which a mean profile is built by the motion of a smaller, approximately rigid, instantaneous profile as detailed in Ref. [25], and outlined in Fig. 5. By describing the local mean profile $J(R, Z) = J(\mathbf{R})$ as the convolution of the instantaneous profile $j(\mathbf{R})$ and a displacement PDF $f(\mathbf{R})$, we describe the temporal average (first moment) $J = J_1$ of a time series at $\mathbf{R}_0$ as the spatial average of $j(\mathbf{R} - \mathbf{R}_0)$ weighed by $f(\mathbf{R})$, which generalizes directly to arbitrary (noncentral) moments of order q [25],

$$J_q(\mathbf{R}_0) = \iint j(\mathbf{R} - \mathbf{R}_0)^q\, f(\mathbf{R})\, dR\, dZ. \tag{3}$$

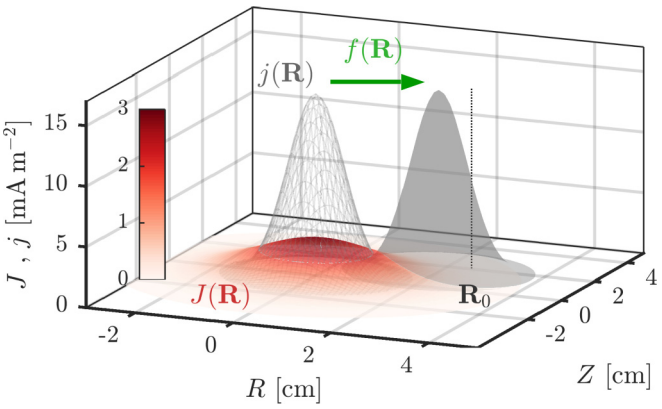

FIG. 5. Schematic of quantities in the analytical model, comprising the mean profile $J(\mathbf{R})$ and smaller instantaneous profile $j(\mathbf{R})$, which is deflected rigidly through the displacement PDF $f(\mathbf{R})$ toward a particular measurement position $\mathbf{R}_0$, where the detector area (aperture) is centered.

A. Subdiffusion

As the simplest scenario, we first approximate both $j(\mathbf{R})$ and $f(\mathbf{R})$ [and therefore the mean profile $J(\mathbf{R})$] as symmetric 2D Gaussians,

$$j(\mathbf{R}) = \frac{I}{2\pi\sigma_j^2} e^{-\frac{(R^2+Z^2)}{2\sigma_j^2}} = j_p\, e^{-\frac{(R^2+Z^2)}{2\sigma_j^2}}, \tag{4}$$

$$f(\mathbf{R}) = \frac{1}{2\pi\sigma_f^2} e^{-\frac{(R^2+Z^2)}{2\sigma_f^2}}, \tag{5}$$

$$\Rightarrow J(\mathbf{R}) = \frac{I}{2\pi\sigma_J^2} e^{-\frac{(R^2+Z^2)}{2\sigma_J^2}}, \tag{6}$$

where σ denotes the respective standard deviations in both the radial and vertical direction and we have $\sigma_J^2 = \sigma_j^2 + \sigma_f^2$. Assuming a total detectable current I, the parameter $j_p = \frac{I}{2\pi\sigma_j^2}$ denotes the peak of the instantaneous current density profile $j(\mathbf{R})$, and hence the maximum in any time series of the profile, pending noise. For such Gaussian profiles, one can obtain a concise analytical expression for the moments J_q,

$$\begin{aligned} J_q(R,Z) &= q^{-1} s_q \rho^{(2-2s_q)} j_p^{(q-s_q)} J(R,Z)^{s_q} \\ \text{with} \quad s_q &= [1-\rho^2(1-q^{-1})]^{-1}, \end{aligned} \tag{7}$$

where the parameter $\rho = \frac{\sigma_j}{\sigma_J}$ denotes the ratio of width of the instantaneous time-average profile. Using Eq. (7), the skewness of any prospective local time series can be predicted solely from the measurement of the mean profile, once the parameters ρ and j_p are set. While they may be given from prior knowledge of the system or extracted from simulations (see [25], Sec. V), we leave them as free parameters for least-squares fitting moments predicted from the model to those of the measured time series. Specifically, to assess the validity of this Gaussian model for each subdiffusive profile, we perform simultaneous least-squares fits with the second

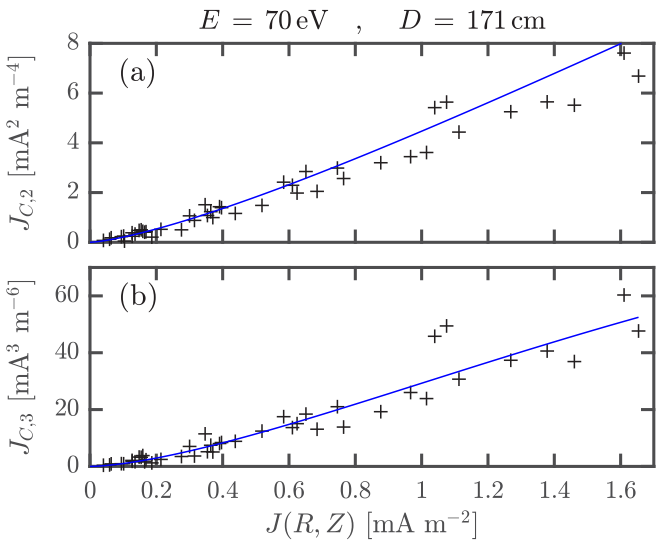

FIG. 6. Fits (blue) of the second (a) and third (b) central moment of the fast ion time series at 70 eV and $D = 171$ cm, as a function of the mean profile value $J(R,Z)$, as detailed on the right-hand side of Eqs. (8) and (9). The crosses represent experimental data points calculated from measurements on each time series as detailed on the left-hand side. The corresponding (normalized) profile is given in Fig. 3(c).

and third *central* moments $J_{C,[2,3]}$,

$$\sigma_{\mathcal{S}}^2 - \sigma_{\mathcal{N}}^2 \approx J_{C,2} = J_2 - J^2, \tag{8}$$

$$\gamma_{\mathcal{S}}\sigma_{\mathcal{S}}^3 - \gamma_{\mathcal{N}}\sigma_{\mathcal{N}}^3 \approx J_{C,3} = J_3 - 3JJ_2 + 2J^3. \tag{9}$$

The right-hand side are the fit functions (Fig. 6, blue) across the data points calculated from measurements as shown on the left-hand side (Fig. 6, crosses). Again, the skewness (γ) and standard deviation (σ) from the ion-source on-phase signals are indicated with $\mathcal{S}$. The second term on the left-hand side removes noise contributions ($\mathcal{N}$), measured during off-phases. We consider all (R,Z) with $J(R,Z) > 0.04$ mA m^{-2}, being twice the typical measurement uncertainty from bootstrap error calculations. Since I enters in a fit parameter, no normalization to common total currents is undertaken. The fit result for $J_{C,[2,3]}$ shown in Fig. 6 demonstrates the potential effectiveness of the method, as the fit appears consistent for the moments of most of the time series considered. Again, it should be noted that the only variable of the fit functions is $J(R,Z)$ itself. To succinctly assess the predictive quality for the skewness (see Fig. 7), we solve for $\gamma_{\mathcal{S}}$ in Eq. (9),

$$\gamma_{\mathcal{S}} \approx \frac{J_{C,3} + \gamma_{\mathcal{N}}\sigma_{\mathcal{N}}^{3/2}}{\left(J_{C,2} + \sigma_{\mathcal{N}}^2\right)^{3/2}}. \tag{10}$$

There is good agreement with measurements, typically within 20%. Larger over- or underestimates [see Fig. 7(a)] may be partly due to temporary fluctuations in the injected fast ion current, which were avoided in more stable settings with lower currents [see Figs. 7(b) and 7(c)]. Comparing with a raw time series in Fig. 2(b), the corresponding $j_p \approx 15$ mA m^{-2} agrees well with the most distinct peaks. Taking I again from integrations, we hence deduce an instantaneous beam width of $\sigma_n \approx 5$ mm, which is consistent with results from numerical

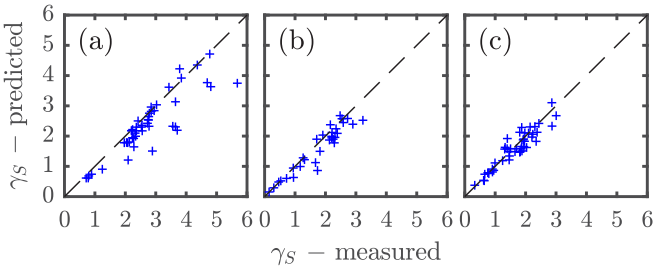

FIG. 7. On-phase skewness γ_S at $D = \{126, 146, 171\}$ cm (a)–(c) for 70 eV profiles as predicted from Eq. (10) vs measured values. The estimated total fast ion currents are $I = \{5.04, 2.97, 2.36\}$ μA.

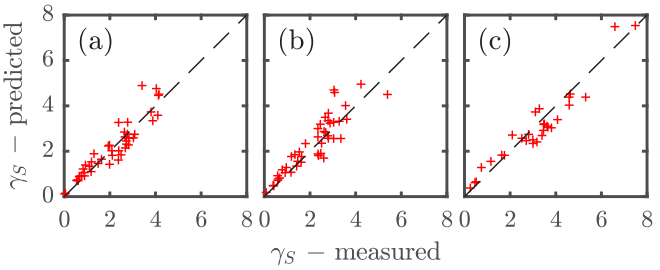

FIG. 8. On-phase skewness γ_S at $D = \{126, 146, 171\}$ cm (a)–(c) for 30 eV profiles as predicted from Eq. (10) [with $J_{C[2,3]}$ from Eqs. (12) and (13)] vs measured values. The estimated total fast ion currents are $I = \{2.35, 2.5, 3.2\}$ μA.

investigations [25]. With a fitted $\rho \geqslant 0.75$, we find, however, that this model provides an underestimated width of the mean profiles by up to a factor of 2. This shows that the features of subdiffusive profiles cannot be entirely reflected by the Gaussian model, despite the accuracy in the fits for moments and skewness. This discrepancy is exacerbated in the larger super- to quasidiffusive profiles, especially since the highest skewness is found in their heavy tails.

B. Super- to quasidiffusion

However, we can reasonably assume a small width of $j(\mathbf{R})$, i.e., $\rho \ll 1$ in this case. This allows us to expand $f(\mathbf{R})$ directly in Eq. (3) as a series about $\mathbf{R}_0$ and find $f(\mathbf{R}) \approx J(\mathbf{R})$ to approximately second order in ρ without any assumptions on the form of $f(\mathbf{R})$. In this limit, one therefore has

$$J_q(R,Z) \approx J(R,Z) \iint n(\mathbf{R})^q \, dR \, dZ + O\left[\frac{\sigma_n^2}{2}\left(\frac{\partial^2 J}{\partial R^2} + \frac{\partial^2 J}{\partial Z^2}\right)\right] \tag{11}$$

and can therefore also find simple analytical expressions for the central moments $J_{C,[2,3]}$ (cf. [25], Sec. IV),

$$J_{C,2} = \tfrac{1}{2} j_p J - J^2, \tag{12}$$

$$J_{C,3} = \tfrac{1}{3} j_p^2 J - \tfrac{3}{2} j_p J^2 + 2J^3 \tag{13}$$

that become our new fit functions in this case. Again, the remaining parameter j_p is left free to perform this simultaneous least-squares fit of predicted $J_{C,[2,3]}$ on the corresponding data points from the time-series measurements, and γ_S is then found according to Eq. (10). Figure 8 shows the resulting γ_S in each super- to quasidiffusive profile.

Again, predictions agree well with measurements, pending noise and fluctuations in the injected current. The fitted j_p follow the trend of total current I across the different profiles, and the value of, e.g., $j_p \approx 14$ mA m^{-2} for $D = 171$ cm corresponds well to the most distinct peaks in the time series of Fig. 2(a). In the 70 eV case, the condition $\rho \ll 1$ stops being valid and thus the Gaussian approximations remain favorable.

In both cases, the presented treatments can be straightforwardly extended to include the fourth-order central moment $J_{C,4}$ and model the kurtosis of the time series. In the cases of less stable injected currents, the more irregularly populated ranges of values of kurtosis become more cumbersome, and relative deviations of measurements from predictions are exacerbated, as expected for higher moments. However, overall good agreement is still found, especially in all fits of the moments and inferred free parameters, so that skewness was chosen again simply as the more concise statistic to present.

V. CONCLUSION

In summary, we have shown experimentally that time intermittency is not exclusive to any particular nondiffusive transport regime for fast ions in TORPEX turbulent plasmas. In this case, it arises from the meandering motion of a concentrated instantaneous fast ion beam, which produces a larger time-average beam. With wider mean profiles toward quasi- and superdiffusion, as well as longer fast ion propagation times, the prevalence of intermittency increases, as instantaneous peaks can become more prominent with respect to the local mean. The ubiquity of intermittency is accurately predicted by an analytical fast ion beam model, which may be of direct interest in similar settings, e.g., in beam physics, and it illustrates the general importance of identifying the system-specific sources of time-intermittent behavior when analyzing nondiffusive transport. Although the specific systems are quite different from our setting, the apparent reduction of the impact of intermittency in situations with increased orbit-averaging (our 70 eV case) could be of interest in other domains in plasma physics, e.g., turbulent fast ion losses in fusion devices [37,38] or the propagation of Solar Energetic Particles [15], as, e.g., for models of SEP dropouts, which feature meandering magnetic flux ropes along which SEPs propagate [39].

ACKNOWLEDGMENTS

We gratefully acknowledge the support of the mechanical, electrical, and electronic workshops at the Swiss Plasma Center. This work has been carried out within the framework of the EUROfusion Consortium, and it has received funding from the Euratom research and training programme 2014–2018 and 2019–2020 under Grant Agreement No. 633053. The views and opinions expressed herein do not necessarily reflect those of the European Commission. This work was partly funded by the Swiss National Science Foundation.

[1] A. F. Hussain, J. Fluid Mech. **173**, 303 (1986).

[2] Z.-S. She, E. Jackson, and S. A. Orszag, Nature (London) **344**, 226 (1990).

[3] P. Davidson, *Turbulence: An Introduction for Scientists and Engineers* (Oxford University Press, Oxford, 2015).

[4] R. Metzler and J. Klafter, Phys. Rep. **339**, 1 (2000).

[5] R. Klages, G. Radons, and I. M. Sokolov, *Anomalous Transport: Foundations and Applications* (Wiley-VCH, Weinheim, 2008).

[6] M. M. Meerschaert and A. Sikorskii, *Stochastic Models for Fractional Calculus*, De Gruyter Studies in Mathematics (De Gruyter, Berlin, Boston, 2011).

[7] E. W. Montroll and G. H. Weiss, J. Math. Phys. **6**, 167 (1965).

[8] R. Metzler and J. Klafter, Phys. Rev. E **61**, 6308 (2000).

[9] F. Alouani-Bibi and J. A. Le Roux, Astrophys. J. **781**, 93 (2014).

[10] D. El Masri, L. Berthier, and L. Cipelletti, Phys. Rev. E **82**, 031503 (2010).

[11] R. L. Martin, D. J. Jerolmack, and R. Schumer, J. Geophys. Res.: Earth **117**, F01018 (2012).

[12] P. Paradisi, R. Cesari, A. Donateo, D. Contini, and P. Allegrini, Nonlin. Proc. Geophys. **19**, 113 (2012).

[13] V. Budaev, S. Takamura, N. Ohno, and S. Masuzaki, Nucl. Fusion **46**, S181 (2006).

[14] A. Bovet, A. Fasoli, and I. Furno, Phys. Rev. Lett. **113**, 225001 (2014).

[15] G. Zimbardo, E. Amato, A. Bovet, F. Effenberger, A. Fasoli, H. Fichtner, I. Furno, K. Gustafson, P. Ricci, and S. Perri, J. Plasma Phys. **81**, 495810601 (2015).

[16] Y. Pomeau and P. Manneville, Commun. Math. Phys. **74**, 189 (1980).

[17] G. Zumofen and J. Klafter, Phys. Rev. E **47**, 851 (1993).

[18] R. Artuso and R. Burioni, in *Large Deviations in Physics* (Springer, Heidelberg, New York, Dodrecht, London, 2014), pp. 263–293.

[19] L. Seuront and H. E. Stanley, Proc. Natl. Acad. Sci. USA **111**, 2206 (2014).

[20] S. H. Müller, A. Diallo, A. Fasoli, I. Furno, B. Labit, and M. Podestà, Phys. Plasmas **14**, 110704 (2007).

[21] A. Fasoli, A. Burckel, L. Federspiel, I. Furno, K. Gustafson, D. Iraji, B. Labit, J. Loizu, G. Plyushchev, P. Ricci, C. Theiler, A. Diallo, S. H. Müller, M. Podestà, and F. Poli, Plasma Phys. Controlled Fusion **52**, 124020 (2010).

[22] I. Furno, F. Avino, A. Bovet, A. Diallo, A. Fasoli, K. Gustafson, D. Iraji, B. Labit, J. Loizu, S. Müller *et al.*, J. Plasma Phys. **81**, 345810301 (2015).

[23] P. Ricci, F. D. Halpern, S. Jolliet, J. Loizu, A. Mosetto, A. Fasoli, I. Furno, and C. Theiler, Plasma Phys. Controlled Fusion **54**, 124047 (2012).

[24] K. Gustafson, P. Ricci, A. Bovet, I. Furno, and A. Fasoli, Phys. Plasmas **19**, 062306 (2012).

[25] M. Baquero-Ruiz, F. Manke, I. Furno, A. Fasoli, and P. Ricci, Phys. Rev. E **98**, 032111 (2018).

[26] M. Baquero-Ruiz, F. Avino, O. Chellai, A. Fasoli, I. Furno, R. Jacquier, F. Manke, and S. Patrick, Rev. Sci. Instrum. **87**, 113504 (2016).

[27] M. Podestà, A. Fasoli, B. Labit, M. McGrath, S. Müller, and F. Poli, Plasma Phys. Controlled Fusion **48**, 1053 (2006).

[28] F. M. Poli, M. Podestà, and A. Fasoli, Phys. Plasmas **14**, 052311 (2007).

[29] B. Labit, I. Furno, A. Fasoli, A. Diallo, S. H. Müller, G. Plyushchev, M. Podestà, and F. M. Poli, Phys. Rev. Lett. **98**, 255002 (2007).

[30] P. Ricci, C. Theiler, A. Fasoli, I. Furno, B. Labit, S. Müller, M. Podestà, and F. M. Poli, Phys. Plasmas **16**, 055703 (2009).

[31] I. Furno, B. Labit, M. Podestà, A. Fasoli, S. H. Müller, F. M. Poli, P. Ricci, C. Theiler, S. Brunner, A. Diallo, and J. Graves, Phys. Rev. Lett. **100**, 055004 (2008).

[32] S. H. Müller, C. Theiler, A. Fasoli, I. Furno, B. Labit, G. R. Tynan, M. Xu, Z. Yan, and J. H. Yu, Plasma Phys. Controlled Fusion **51**, 055020 (2009).

[33] C. Theiler, I. Furno, P. Ricci, A. Fasoli, B. Labit, S. H. Müller, and G. Plyushchev, Phys. Rev. Lett. **103**, 065001 (2009).

[34] G. Plyushchev, A. Diallo, A. Fasoli, I. Furno, B. Labit, S. H. Müller, M. Podestà, F. M. Poli, H. Boehmer, W. W. Heidbrink, and Y. Zhang, Rev. Sci. Instrum. **77**, 10F503 (2006).

[35] A. Bovet, A. Fasoli, P. Ricci, I. Furno, and K. Gustafson, Phys. Rev. E **91**, 041101(R) (2015).

[36] R. Shanmugam and R. Chattamvelli, *Statistics for Scientists and Engineers* (Wiley Online, 2015).

[37] W. Heidbrink and G. Sadler, Nucl. Fusion **34**, 535 (1994).

[38] A. Fasoli, C. Gormenzano, H. Berk, B. Breizman, S. Briguglio, D. Darrow, N. Gorelenkov, W. Heidbrink, A. Jaun, S. Konovalov *et al.*, Nucl. Fusion **47**, S264 (2007).

[39] T. Laitinen, A. Kopp, F. Effenberger, S. Dalla, and M. Marsh, Astron. Astrophys. **591**, A18 (2016).